Article

Chinese Science Bulletin

Electron Physics

June 2012 Vol.57 No.17: 2087–2093
doi: 10.1007/s11434-012-5105-3

Comparative investigation of three types of ethanol sensor based on NiO-SnO_2 composite nanofibers

SHEN RenSheng[1*], LI XiangPing[1], XIA XiaoChuan[1], LIANG HongWei[1], WU GuoGuang[2], LIU Yang[1], CHENG ChuanHui[1] & DU GuoTong[1,2*]

[1] *School of Physics and Optoelectronic Technology, Dalian University of Technology, Dalian 116024, China;*
[2] *State Key Laboratory on Integrated Optoelectronics, College of Electronic Science and Engineering, Jilin University, Changchun 130012, China*

Received October 23, 2011; accepted December 12, 2011

NiO-SnO_2 composite nanofibers were synthesized via electrospinning techniques and characterized by X-ray diffraction, scanning electron microscopy, transmission electron microscopy, and X-ray photoelectron spectroscopy. Three types of sensor were applied to investigate the sensing properties of these nanofibers. Sensors A were fabricated by mixing the nanofibers with deionized water, and then grinding and coating them on ceramic tubes to form indirect heated gas sensors. Microsensors B (with an area of 600 μm×200 μm) were formed by spinning nanofibers on Si substrates with Pt signal electrodes and Pt heaters. Sensors C were fabricated by spinning nanofibers on plane ceramic substrates (with a large area of 13.4 mm×7 mm) with Ag-Pd signal electrodes only. The operating temperatures of sensors A and B were controlled by adjusting heater currents, and the operating temperatures of sensors C were controlled by adjusting an external temperature control device. Experimental results show that sensors C possess the highest sensing properties, such as high response values (about 42 to 100 μL/L ethanol), quick response/recovery speeds (the response and recovery times were 4 and 7 s, respectively), and excellent consistencies. These phenomena were explained by the retained fiber morphology and suitable sensor area. The presented results can provide some useful information for the design and optimization of one-dimensional nanomaterial-based gas sensors.

SnO_2, semiconductors, electrospinning, nanofibers, gas sensors

Citation: Shen R S, Li X P, Xia X C, et al. Comparative investigation of three types of ethanol sensor based on NiO-SnO_2 composite nanofibers. Chin Sci Bull, 2012, 57: 2087–2093, doi: 10.1007/s11434-012-5105-3

Chemical gas sensors have found wide applications in industrial production, environmental monitoring and protection [1–3]. Many of these sensors are fabricated by loading metal-oxide semiconductor (MOS) materials as the sensing materials, such as SnO_2 [2], ZnO [4], WO_3 [3], In_2O_3 [5], and NiO [6]. The sensor performances are strongly dependent on the morphology and structure of MOS, namely, grain size, surface area and dimension, as well as the type of grain network or porosity [7]. Traditional MOS sensing materials are nanoparticles/nanopowders [8], which have advantages in volume-production, complex doping, and low-cost fabrication. However, these materials often suffer from degradation because of the aggregation growth among nanoparticles/nanopowders [9]. In recent years, one-dimensional (1D) MOS nanomaterials have received considerable attention because they can avoid such degradation [10,11]. Simultaneously, the high surface-to-volume ratios of 1D nanomaterials can provide more sites for analyte molecule adsorption, leading to high response values and short response/recovery times [12]. Moreover, their large length-to-diameter characteristic can also cause charge carriers to traverse the barriers introduced by molecular recognition [13]. Many scientists agree that these novel materials are expected to replace traditional nanoparticles and nanopowders, and be widely chosen to fabricate microsensors or nanosensors [14–16].

Several types of sensors have been employed to investigate the sensing properties of 1D nanomaterials. A typical

*Corresponding authors (email: dugt@dlut.edu.cn; shjiank@dlut.edu.cn)

strategy is to fabricate indirect heated gas sensors with 1D nanomaterials for testing [17–19]. This method is simple, convenient, and only requires standard equipment (e.g. agate mortars and coating pens). Indirect heated gas sensors have been investigated for more than forty years. Such technology is well developed in laboratories and factories, and is regularly chosen by many research groups for 1D nanomaterial-based sensing investigation (especially in China). Another method involves integrating material synthesis and sensor fabrication to fabricate microsensors or nanosensors. These sensors usually have plane surfaces for depositing sensing materials, and their surface areas range from several μm^2 to many cm^2 [20–22]. A large amount of sensing results from 1D nanomaterial-based sensors have been reported to date; however, the influence of sensor type on the sensing results has not so far been considered.

This paper presents the sensing properties of three types of sensor loading the same sensing material. NiO-SnO_2 composite nanofibers synthesized via electrospinning are used in our experiment for their typicality as 1D nanomaterials. SnO_2 is a highly sensitive material for the detection of both reducing and oxidizing gases [12]. NiO is a traditional dopant with p-type properties, which can enhance the sensing performance of n-type material greatly [12]. Electrospinning is a unique technique offering a relatively easy and versatile method for the large-scale synthesis of 1D nanostructures that are exceptionally long in length, uniform in diameter, large in surface area, and diversified in composition [23–25]. Sensors with different structures were fabricated and compared in detail. We consider that the obtained results will be useful for sensor design and optimization.

1 Experimental

The electrospinning process in the present experiment was similar to the process described previously for SnO_2 nanofiber synthesis [25]. All the chemicals were of analytical grade and purchased from Tianjin Guangfu Fine Chemical Research Institute (Tianjin, China). Typically, 0.5 g of tin dichloride was mixed with 5.0 g of *N*,*N*-dimethylformamide (DMF), 0.1 g of $NiCl_2 \cdot 6H_2O$, and 5.0 g of ethanol in a glovebox under vigorous stirring for 6 h. Subsequently, this solution was added to 1.0 g of poly(vinyl pyrrolidone)(PVP) under vigorous stirring for 10 h. Then, the mixture was loaded into a glass syringe and connected to a high-voltage power supply. A voltage of 10 kV was applied between the cathode (a flat aluminum foil) and anode (syringe) at a distance of 20 cm to obtain fiber precursors. The conversion of the fiber precursors to NiO-SnO_2 composite nanofibers and the removal of PVP from the as-spun nanofibers were achieved by calcining the fibers at 600°C for 3 h in air.

Sensors A were indirect heated sensors, and the fabrication details can be found in many previous papers [17–19]. Briefly, the as-calcined nanofibers were mixed and ground (about 3 min) with deionized water in a weight ratio of 100∶25 to form a paste. The paste was coated on ceramic tubes (outside d=1.35 mm, l=6 mm) on which two Au signal electrodes were previously printed (the distance between signal electrodes was about 2 mm). Ni-Cr heating wires (d=0.5 mm, R=35 Ω at room temperature) were inserted in the ceramic tubes as heaters. Figure 1(a) shows a photograph of the ceramic tubes and Ni-Cr heaters on a sensor socket, and a schematic for the structure of sensors A is also inserted in this figure. The performances of sensors A were measured using a CGS-8 (chemical gas sensor-8) intelligent gas sensing analysis system (Beijing Elite Tech Co., Ltd, China) (Figure 1(b)). This system could provide various operating currents to control the sensor temperature (measured using a Testo 845 infrared thermometer (TESTO AG, Germany).

Sensors B were microsensors [26–28], and the microsensor substrates were fabricated according to the following steps: (a) a layer of SiO_2 (thickness of 2000 Å) was grown on the two sides of Si-substrates as an insulating layer, (b) a platinum layer (thickness of 1800 Å) was then sputtered on the SiO_2 layers as metal electrodes, (c) mask patterns were then transferred to the Si wafer by photolithography, (d) the platinum layers were then etched to form signal electrodes and heater electrodes by reactive ion etching, (e) the photoresist was then removed. The top view (obtained using an optical microscope) and the electrode design of the as-fabricated sensors B is shown in Figure 1(c). The electrode width was 20 μm, and the sensor area was 600 μm×200 μm. Sensing films were deposited on sensors B by laying sensor substrates on the aluminum foil using the electrospinning process by spinning the substrates for about 6 h, and then calcining the electrospun sensing films at 600°C for 3 h. The Si substrates were then sandwiched between signal electrodes and heater electrodes to afford a type of sensors reported as sandwich-structure microsensors [26,27]. The testing instrument used for sensors B was the same as that for sensors A (Figure 1(d)).

Sensors C were plane sensors with large areas (13.4 mm ×7 mm) [29]. These sensors were fabricated by screen-printing Ag-Pd pastes on ceramic substrates and then calcining the screen-printed pastes at 900°C for 5 h. The top view and the electrode design of sensors C are shown in Figure 1(e). The depositing process of nanofibers on sensors C was the same as that for sensors B. As Ag-Pd electrodes could not be applied in sensors C as heaters because of their low stability, we used a testing system with an external temperature control to adjust the operating temperature (CGS-1TP, chemical gas sensor-1 temperature pressure, shown in Figure 1(f)). This system could conductively adjust the sensor temperature from room temperature to about 500°C with a precision of 1°C.

Gas sensing properties were measured by using a static test system [18,19,21]. All the sensors were pre-heated at

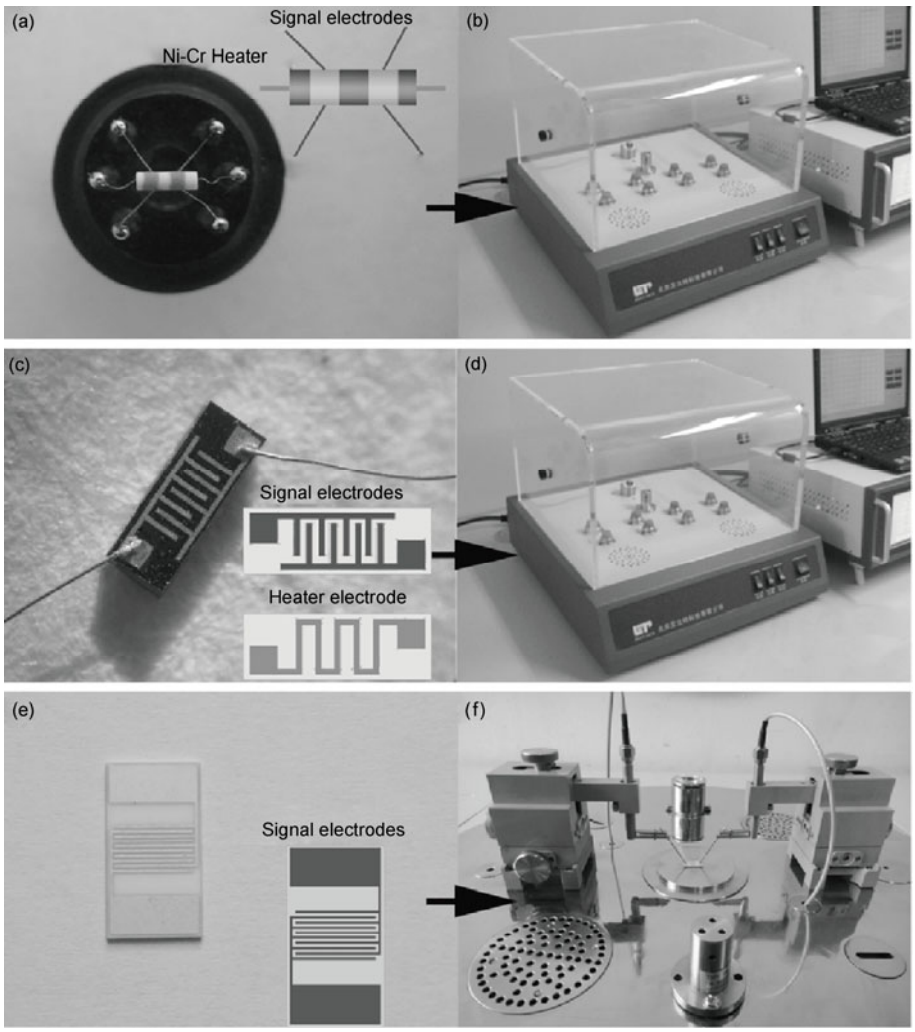

Figure 1 Photographs of sensors A (a), sensors A in CGS-8 gas sensing analysis system (b), sensors B (c), sensors B in CGS-8 gas sensing analysis system (d), sensors C (e), and sensors C in CGS-1TP gas sensing analysis system (f).

different operating temperatures (or currents) for about 30 min. When the resistances of the sensors were stable, saturated target gas was injected into the test chamber (20 and 18 L in volume for CGS-8 and CGS-1TP respectively) by a micro-injector through a rubber plug. The saturated target gas was mixed with air by two fans in the analysis system. After the sensor resistances reached new constant values, the test chamber was opened to recover the sensors in air. The whole experiment process was performed in a super-clean room with the constant humidity (25% relative humidity) and temperature (20°C), which were also monitored by the analysis systems.

The response value (R) was designated as $R = R_a/R_g$, where R_a was the sensor resistance in air (base resistance) and R_g was a mixture of target gas and air. The time taken by the sensor resistance to change from R_a to R_a–90%×(R_a–R_g) was defined as response time when the target gas was introduced to the sensor, and the time taken from R_g to R_g+90%×(R_a–R_g) was defined as recovery time when the ambience was replaced by air.

Scanning electron microscopy (SEM) images were recorded on a SHIMADZU SSX-550 (Japan) instrument. Transmission electron microscopy (TEM) images were obtained on a HITACHI S-570 microscope with an accelerating voltage of 200 kV. X-ray powder diffraction (XRD) data were collected on an X'Pert MPD Philips diffractometer (Cu Kα X-radiation at 40 kV and 50 mA). Sample compositions and chemical states were confirmed by X-ray photoelectron spectroscopy (XPS, SPECS XR50) with an MgKα X-ray source (1253.6 eV). The binding energy in XPS spectrum was calibrated with C 1s peak of 284.6 eV.

2 Results and discussion

Figure 2(a) displays the XRD pattern obtained from the as-calcined products. The prominent peaks corresponding to (110), (101) and (211) crystal planes and all other smaller peaks (such as (200), (220), (310), and (301)) coincide with the corresponding peaks of the rutile structure of SnO_2 given

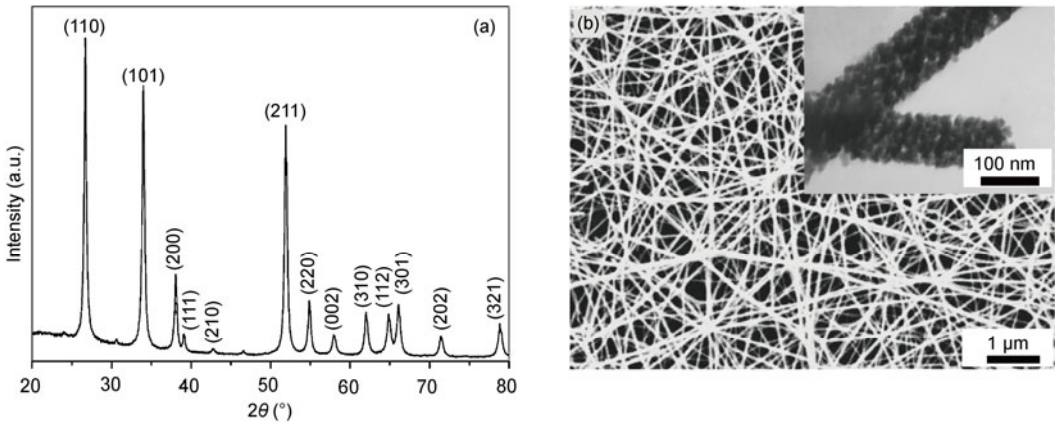

Figure 2 XRD pattern (a) and a SEM image (b) of NiO-SnO_2 composite nanofibers. The insert shows a TEM image.

in the standard data file (JCPDS file no.41-1445) [30]. No diffraction peaks from NiO are detected, which is because of the very low amount of NiO in the SnO_2 nanofibers [25]. Figure 2(b) shows the SEM image of the calcined products. Many nanofibers with diameters ranging from 80 to 190 nm and lengths of several tens of micrometers can be found. The average diameter of these nanofibers is around 120 nm. The insert in Figure 2(b) is a TEM image of the nanofibers, which shows that the nanofibers are formed by well-regulated nanoparticles with an average diameter of about 15 nm.

Figure 3(a) shows the wide XPS spectrum of the nanofibers. Figure 3(b)–(d) show close up views of the Sn 3d, Ni 2p and O 1s XPS spectra, respectively. The dominated peak of Sn 3d located at 486.05 eV can be assigned to Sn^{4+}, meaning SnO_2 formation. The Ni $2p_{3/2}$ peak was observed at 855.72 eV in Figure 3(c), and was accompanied by a satellite peak at 861.39 eV, implying the presence of a high-spin Ni^{2+} [31–33]. Concerning the O 1s XPS spectrum, it can be divided into two components located at 529.89 and 530.76 eV, respectively, corresponding to Sn–O and Ni–O bonds. The results demonstrate that the sample was composed of SnO_2 and NiO. The atomic ratio of O, Sn and Ni is calculated to be 62.322∶32.266∶5.412.

The sensors were exposed to 100 μL/L ethanol at different operating temperatures to find the optimum conditions. As shown in Figure 4, all samples exhibit the maximum responses at 300°C, which can be explained by considering the same nanofiber loading. Below 300°C, the lower

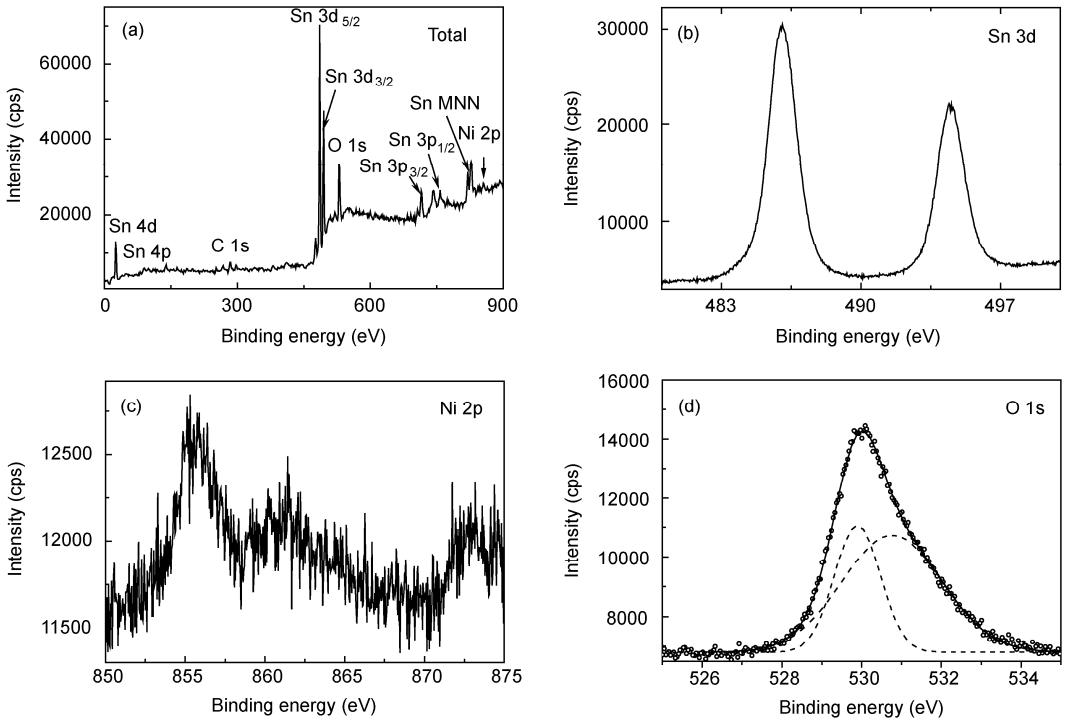

Figure 3 XPS spectra of the as-calcined nanofibers: total spectrum (a), Sn 3d peak (b), Ni 2p peak (c) and O 1s peak (d).

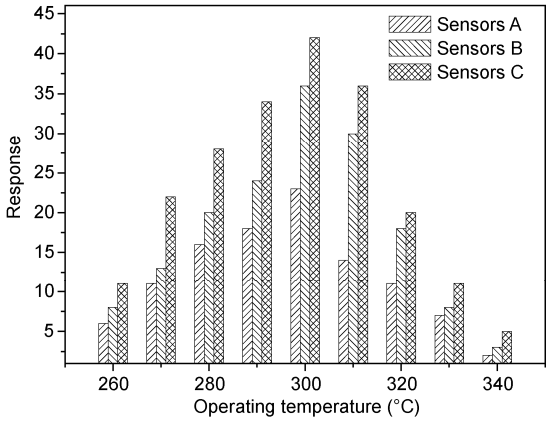

Figure 4 Responses of sensors A, B, and C to 100 μL/L ethanol at different operating temperatures.

responses are based on the weak activation of the oxygen species on the SnO_2 surface. While at exorbitant high temperatures (above 300°C), the decreased responses are due to fewer molecules that can be absorbed with high activation [7]. Besides, the surface coverage of oxygen adsorbates at the steady-state is also dependent on the temperature. A suitable operating temperature can enhance the amounts of oxygen adsorbates at the steady-state, thus leading to a higher response [7]. At the optimum operating temperature of 300°C, sensors A show a small response (about 23), while sensors B and C show much higher values (36 and 42 respectively).

Response-recovery curves can reveal the reacting speeds between target gas molecules and the surface oxygen species. Previous papers discussed that 1D nanomaterials showed fast response and recovery speeds, which were due to the high surface-to-volume ratios, while the web-like structures of these materials could easily absorb and desorb gas molecules [13]. Similar results are also found in our investigation. As seen in Figure 5, the response and recovery times of sensors A are about 9 and 10 s, respectively, which are shorter than those of many nanoparticles or nanopowders-based sensors. However, sensors B and C show similar and enhanced reaction speeds, and the corresponding response and recovery times are 4 and 7 s, respectively.

Furthermore, the sensors are exposed to different concentrations of ethanol to reveal the distinction of response values based on various investigating methods. Each type of sensor shows increasing response values with enhancing gas concentrations (Figure 6), but sensors A exhibit the lowest values in all the tests. For instance, the response of sensors A is only 80 to 1000 μL/L ethanol, while the response values of sensors B and C are 141 and 183 μL/L ethanol, respectively.

We have fabricated ten sensors for each sensor type. The results in Figures 4–6 are based on the sensors with medium performances. Figure 7 shows the responses of all these 10 sensors to 100 μL/L ethanol at 300°C. It can be found that sensors A and B possess poor consistencies, while sensors C show an improved and excellent consistency, which directly confirms the advantage of sensors C in sensing investigation.

Based on the above results, we confirm that sensors A

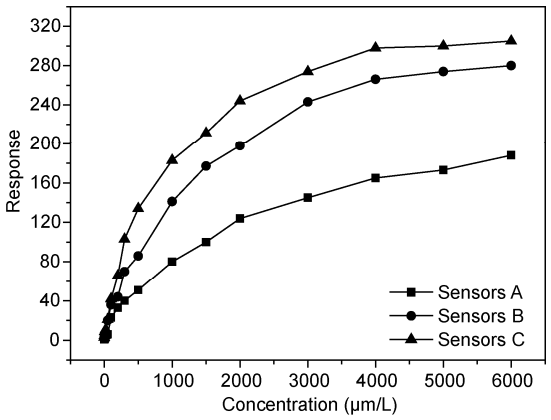

Figure 6 Responses of sensors A, B, and C to different concentrations of ethanol at 30°C.

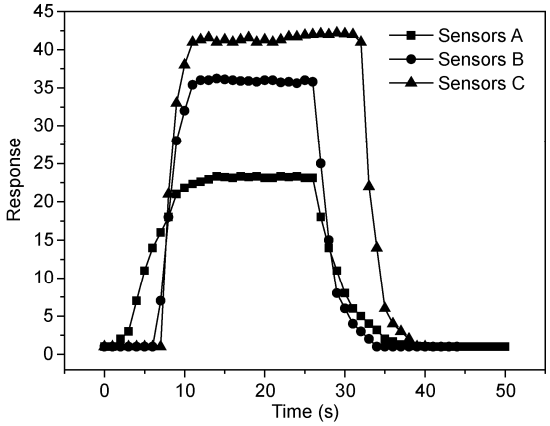

Figure 5 Response-recovery curves of sensors A, B, and C to 100 μL/L ethanol at 300°C.

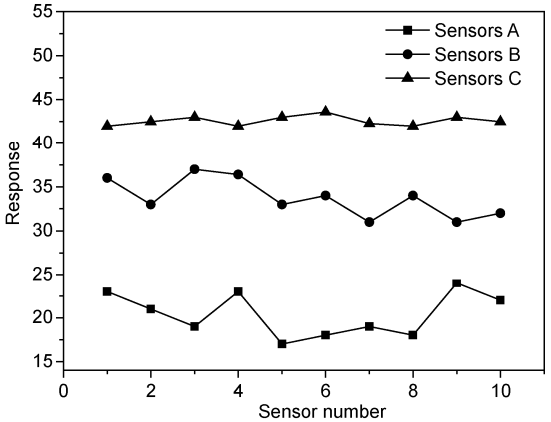

Figure 7 Consistency of sensors A, B, and C to 100 μL/L ethanol at 300°C.

show the lowest response values, the longest response or recovery times, and the poorest consistency. Sensors B and C exhibit similar results in response value and reaction speed tests, but sensors C have an advantage in consistency. The explanation of these phenomena is discussed as follows.

The sensing mechanism of SnO_2 or similar semiconductor-based gas sensors has been clarified in many previous works [7]. The most widely accepted model is that the resistance change of the SnO_2 gas sensors is primarily caused by the adsorption and desorption of gas molecules on the material surface. When SnO_2 is surrounded by air, oxygen molecules will be adsorbed on the SnO_2 surface to generate chemisorbed oxygen species (O_2^-, O^{2-}, O^-, and O^- is believed to be dominant [34]), and thus SnO_2 will show a high resistance. When ethanol is introduced at moderate temperature, SnO_2 is exposed to the traces of reductive gas. By reacting with the oxygen species on the SnO_2 surface, the reductive ethanol molecules will reduce the concentration of oxygen species on the SnO_2 surface and thus increase the electron concentration, which eventually increases the conductivity of the SnO_2 sensors. NiO is a p-type semiconductor. According to Jain et al. [35], this material can be segregated over the n-type SnO_2, forming n-p junctions. It has been reported that with sensing materials composed of two successive bodies A and B whose conductivity types are different such as p- and n-type, under certain conditions, high response and good selectivity can be observed [36]. When the sensors are exposed to a target atmosphere, the chemical species to be detected in the atmosphere can permeate into the interface of the p-n junction, and lead to changes in electrical properties at the junction. The sensing mechanism of many p-n type materials such as CuO-ZnO and CuO-SnO_2 are all related to this model [12].

To explain the effect of sensor types on their performances, the material morphology and sensor structure should be considered. The lowest response values, longest response/recovery times, and poorest consistency of sensors A are directly related to the destroyed fiber morphology on this type of sensor. As shown in Figure 8, all the nanofibers have been broken during the grinding and coating process for sensors A, and this demolishment will surely lead to the decreased sensing properties. The poor consistency of sensors A can be explained by the uncontrollable thickness of the sensing films on the ceramic tubes, which is resulted from a hand-worked coating. Sensors B and C show many similar characteristics for the same deposition methods used. However, their consistencies are quite different. We consider that this is due to the difference in area between the two sensors. As shown in Figure 9, deposition of the nanofibers during electrospinning is uneven [23], and a sensor individuality will result with a smaller area. To test our hypothesis, we recorded all the original resistances (R_g) of sensors B and C at 300°C. The results in Figure 10 show that sensors C own a flat resistance curve, while sensors B exhibit many fluctuant values. The fluctuant R_g of sensors B corresponds to an inhomogeneous film distribution and thickness, thus resulting in the eventual poor consistency in the tests.

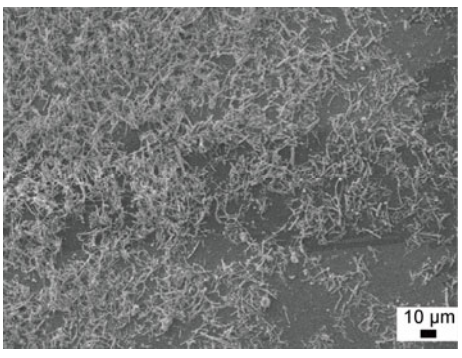

Figure 8 A SEM image of NiO-SnO_2 composite nanofibers coated on sensors A.

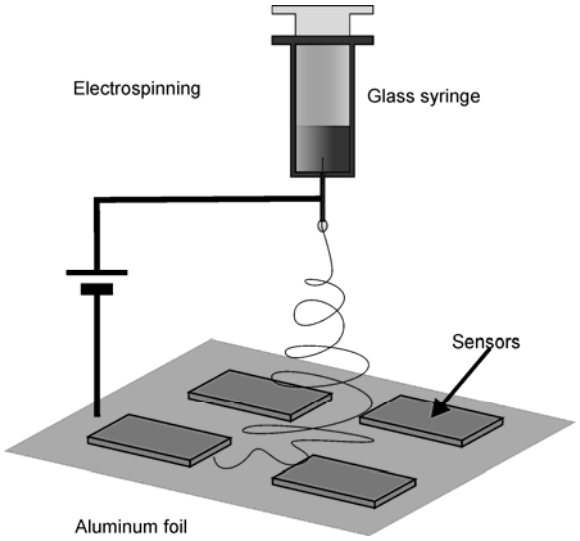

Figure 9 Schematic diagram of the depositing distribution for sensors B and C.

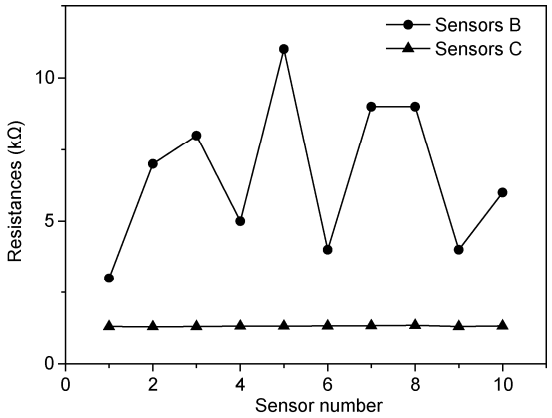

Figure 10 Original resistances (R_g) of sensors B and C at 300°C.

3 Conclusions

In summary, three types of sensor were fabricated using the same sensing material of NiO-SnO_2 composite nanofibers. The results show that the fabrication process for indirect heated gas sensors destroys the nanofiber morphology, and is therefore not suitable for investigation on 1D sensing nanomaterials. Using plane sensors can preserve the fiber morphology because no grinding or coating processes are needed; thus sensors B and C show enhanced sensing properties. However, as the deposition of nanofibers during electrospinning is uneven, the sensor area should also be considered in the design of microsensors.

This work was supported by the National High Technology Research and Development Program of China (2009AA03Z401), the Scientific Research Foundation for Doctoral Program of Liaoning Province of China (20101016) and Research Fund for the Doctoral Program of Higher Education of China (20110041120045).

1 Janata J, Josowicz M, Devaney D M. Chemical sensors. Anal Chem, 1994, 66: 207–228
2 Liu L, Zhang T, Li S C, et al. Micro-structure sensors based on ZnO microcrystals with contact-controlled ethanol sensing. Chin Sci Bull, 2009, 54: 4371–4375
3 Lei H, Yi L. Improved acetone sensing properties of flat sensors based on Co-SnO_2 composite nanofibers. Chin Sci Bull, 2011, 56: 2644–2648
4 Albert S, Viricelle J P, Tournier G, et al. Detection of oxygen traces in nitrogen- and hydrogen-rich atmosphere. Sens Actuator B-Chem, 2009, 139: 298–303
5 Ali M, Wang C Y, Röhlig C C, et al. NO_x sensing properties of In_2O_3 thin films grown by MOCVD. Sens Actuator B-Chem, 2008, 129: 467–472
6 Plashnitsa V V, Ueda T, Elumalai P, et al. Zirconia-based planar NO_2 sensor using ultrathin NiO or laminated NiO-Au sensing electrode. Ionics, 2008, 14: 15–25
7 Barsan N, Koziej D, Weimar U. Metal oxide-based gas sensor research: How to? Sens Actuator B-Chem, 2007, 121: 18–35
8 Neri G, Bonavita A, Micali G, et al. Resistive CO gas sensors based on In_2O_3 and $InSnO_x$ nanopowders synthesized via starch-aided sol-gel process for automotive applications. Sens Actuator B-Chem, 2008, 132: 224–233
9 Sahm T, Mädler L, Gurlo A, et al. Flame spray synthesis of tin dioxide nanoparticles for gas sensing. Sens Actuator B-Chem, 2004, 98: 148–153
10 Kong J, Franklin N R, Zhou C, et al. Nanotube molecular wires as chemical sensors. Science, 2000, 287: 622–625
11 Qi P, Vermesh O, Grecu M, et al. Toward large arrays of multiplex functionalized carbon nanotube sensors for highly sensitive and selective molecular detection. Nano Lett, 2003, 3: 347–351
12 Franke M E, Koplin T J, Simon U. Metal and metal oxide nanoparticles in chemiresistors: Does the nanoscale matter? Small, 2006, 2: 36–50
13 Kolmakov A, Moskovits M. Chemical sensing and catalysis by one-dimensional metal-oxide nanostructures. Annu Rev Mater Res, 2004, 34: 151–180
14 Hao R C, Li D C. Theoretical and experimental study on magnetic-fluid-based flow sensors. Chin Sci Bull, 2011, 56: 1844–1847
15 Li J J, Zhang X T, Chen Y H, et al. Synthesis of highly ordered SnO_2/Fe_2O_3 composite nanowires arrays by electrophoretic deposition method. Chin Sci Bull, 2005, 50: 1044–1047
16 Zhu B L, Sui Z M, Chen X, et al. Synthesis of gold-doped TiO_2 nanotubes. Chin Sci Bull, 2005, 50: 711–713
17 Ge J P, Wang J, Zhang H X, et al. High ethanol sensitive SnO_2 microspheres. Sens Actuator B-Chem, 2006, 113: 937–943
18 Liang Y X, Chen Y J, Wang T H. Low-resistance gas sensors fabricated from multiwalled carbon nanotubes coated with a thin tin oxide layer. Appl Phys Lett, 2004, 85: 666–668
19 Qi Q, Zhang T, Liu L, et al. Selective acetone sensor based on dumbbell-like ZnO with rapid response and recovery. Sens Actuator B-Chem, 2008, 134: 166–170
20 Kuang Q, Lao C, Wang Z L, et al. High-sensitivity humidity sensor based on a single SnO_2 nanowire. J Am Chem Soc, 2007, 129: 6070–6071
21 Li Q H, Liang Y X, Wan Q, et al. Oxygen sensing characteristics of individual ZnO nanowire transistors. Appl Phys Lett, 2004, 85: 6389–6391
22 Kolmakov A, Zhang Y, Cheng G, et al. Detection of CO and O_2 using tin oxide nanowire sensors. Adv Mater, 2005, 15: 977–1000
23 Greiner A, Wendorff J H. Electrospinning: A fascinating method for the preparation of ultrathin fibers. Angew Chem Int Ed, 2007, 46: 5670–5703
24 Kim S K, Hwang S H, Chang D, et al. Preparation of mesoporous In_2O_3 nanofibers by electrospinning and their application as a CO gas sensor. Sens Actuator B-Chem, 2010, 149: 28–33
25 Zhang H, Li Z, Liu L, et al. Enhancement of hydrogen monitoring properties based on Pd-SnO_2 composite nanofibers. Sens Actuator B-Chem, 2010, 147: 111–115
26 Lee S M, Dyer D C, Gardner J W. Design and optimization of a high-temperature silicon micro-hotplate for nanoporous palladium pellistors. Microelectron J, 2003, 34: 115–126
27 Gall M. The Si planar pellistor: A low-power pellistor sensor in Si thin-film technology. Sens Actuator B-Chem, 1991, 4: 533–538
28 Zhang T, Liu L, Qi Q, et al. Development of microstructure In/Pd-doped SnO_2 sensor for low-level CO detection. Sens Actuator B-Chem, 2009, 139: 287–291
29 Zhang D, Liu Z, Li C, et al. Detection of NO_2 down to ppb levels using individual and multiple In_2O_3 nanowire devices. Nano Lett, 2004, 4: 1919–1924
30 Epifani M, Comini E, Díaz R, et al. Oxide nanopowders from the low-temperature processing of metal oxide sols and their application as gas-sensing materials. Sens Actuator B-Chem, 2006, 118: 105–109
31 Vasilkov A Y, Nikolaev S A, Smirnov V V, et al. An XPS study of the synergetic effect of gold and nickel supported on SiO_2 in the catalytic isomerization of allylbenzene. Mendeleev Commun, 2007, 17: 268–270
32 Khyzhun O, Sygellou L, Ladas S. Interfacial oxidation of ultrathin nickel and chromium films on yttria-stabilized zirconia. J Phys Chem B, 2005, 109: 2302–2306
33 Liu X F, Yu R H. Mediation of room temperature ferromagnetism in Co-doped SnO nanocrystalline films by structural defects. J Appl Phys, 2007, 102: 083917
34 Windischmann H, Mark P. A model for the operation of a thin films tin oxide conductance modulation carbon monoxide sensor. J Electrochem Soc, 1979, 126: 627–630
35 Jain K, Pant R P, Lakshmikumar S T. Effect of Ni doping on thick film SnO_2 gas sensor. Sens Actuator B-Chem, 2006, 113: 823–829
36 Baek K K, Tuller H L. Electronic characterization of ZnO/CuO heterojunctions. Sens Actuator B-Chem, 1993, 13: 238–240